The National Spherical Torus Experiment (NSTX) Research Program and Progress Towards High Beta, Long Pulse Operating Scenarios

E.J. Synakowski[1], M.G. Bell[1], R.E. Bell[1], T. Bigelow[2], M. Bitter[1], W. Blanchard[1], J. Boedo[3], C. Bourdelle[4], C. Bush[2], D.S. Darrow[1], P.C. Efthimion[1], E.D. Fredrickson[1], D.A. Gates[1], M. Gilmore[5], L.R. Grisham[1], J.C. Hosea[1], D.W. Johnson[1], R. Kaita[1], S.M. Kaye[1], S. Kubota[6], H.W. Kugel[1], B.P. LeBlanc[1], K. Lee[7], R. Maingi[2], J. Manickam[1], R. Maqueda[8], E. Mazzucato[1], S.S. Medley[1], J. Menard[1], D. Mueller[1], B.A. Nelson[9], C. Neumeyer[1], M. Ono[1], F. Paoletti[10], H.K. Park[1], S.F. Paul[1], Y.-K. M. Peng[2], C.K. Phillips[1], S. Ramakrishnan[1], R. Raman[9], A.L. Roquemore[1], A. Rosenberg[1], P.M. Ryan[2], S.A. Sabbagh[10], C.H. Skinner[1], V. Soukhanovskii[1], T. Stevenson[1], D. Stutman[11], D.W. Swain[2], G. Taylor[1], A. Von Halle[1], J. Wilgen[2], M. Williams[1], J.R. Wilson[1], X. Xu[12], S.J. Zweben[1], R. Akers[13], R.E. Barry[2], P. Beiersdorfer[12], J.M. Bialek[10], B. Blagojevic[11], P.T. Bonoli[14], R. Budny[1], M.D. Carter[2], J. Chrzanowski[1], W. Davis[1], B. Deng[7], E.J. Doyle[15], L. Dudek[1], J. Egedal[14], R. Ellis[1], J.R. Ferron[15], M. Finkenthal[11], J. Foley[1], E. Fredd[1], A. Glasser[8], T. Gibney[1], R.J. Goldston[1], R. Harvey[16], R.E. Hatcher[1], R.J. Hawryluk[1], W. Heidbrink[17], K.W. Hill[1], W. Houlberg[2], T.R. Jarboe[9], S.C. Jardin[1], H. Ji[1], M. Kalish[1], J. Lawrance[18], L.L. Lao[15], K.C. Lee[7], F.M. Levinton[19], N.C. Luhmann[7], R. Majeski[1], R. Marsala[1], D. Mastravito[1], T.K. Mau[3], B. McCormack[1], M.M. Menon[2], O. Mitarai[20], M. Nagata[21], N. Nishino[22], M. Okabayashi[1], G. Oliaro[1], D. Pacella[23], R. Parsells[1], T. Peebles[6], B. Peneflor[15], D. Piglowski[15], R. Pinsker[15], G.D. Porter[12], A.K. Ram[14], M. Redi[1], M. Rensink[12], G. Rewoldt[1], J. Robinson[1], P. Roney[1], M. Schaffer[15], K. Shaing[24], S. Shiraiwa[25], P. Sichta[1], D. Stotler[1], B.C. Stratton[1], Y. Takase[25], X. Tang[8], R. Vero[11], W.R. Wampler[26], G.A. Wurden[8], X.Q. Xu[12], J.G. Yang[27], L. Zeng[6], W. Zhu[6]

First author e-mail address: synakowski@pppl.gov

[1] Princeton Plasma Physics Laboratory, Princeton University, Princeton, New Jersey, United States of America
[2] Oak Ridge National Laboratory, Oak Ridge, Tennessee, United States of America
[3] University of California, San Diego, California, United States of America
[4] CEA Cadarache, France
[5] University of New Mexico at Albuquerque
[6] University of California, Los Angeles, California, United States of America
[7] University of California, Davis, California, United States of America
[8] Los Alamos National Laboratory, Los Alamos, New Mexico, United States of America
[9] University of Washington, Seattle, Washington, United States of America
[10] Columbia University, New York, N.Y., United States of America
[11] Johns Hopkins University, Baltimore, Maryland, United States of America
[12] Lawrence Livermore National Laboratory, Livermore, California, United States of America
[13] Euratom-UKAEA Fusion Association, Abingdon, Oxfordshire, United Kingdom
[14] Massachusetts Institute of Technology, Cambridge, Massachusetts, United States of America
[15] General Atomics, San Diego, California, United States of America
[16] Compx, Del Mar, California, United States of America
[17] University of California, Irvine, California, United States of America
[18] Princeton Scientific Instruments, Princeton, New Jersey, United States of America
[19] Nova Photonics, Princeton, New Jersey, United States of America
[20] Kyushu Tokai University, Kumamoto, Japan
[21] Himeji Institute of Technology, Okayama, Japan
[22] Hiroshima University, Hiroshima, Japan
[23] ENEA, Frascati, Italy
[24] University of Wisconsin, Madison, Wisconsin, United States of America
[25] Tokyo University, Tokyo, Japan
[26] Sandia National Laboratories, Albuquerque, New Mexico, United States of America
[27] Korea Basic Science Institute, Taejon, Republic of Korea

Abstract - A major research goal of the National Spherical Torus Experiment is establishing long-pulse, high beta, high confinement operation and its physics basis. This research has been enabled by facility capabilities developed over the last two years, including neutral beam (up to 7 MW) and high harmonic fast wave heating (up to 6 MW), toroidal fields up to 6 kG, plasma currents up to 1.5 MA, flexible shape control, and wall preparation techniques. These capabilities have enabled the generation of plasmas with $<\beta_T>$ up to 35%. Normalized beta values often exceed the no wall limit, and studies suggest that passive wall mode stabilization is enabling this for broad pressure profiles characteristic of H mode plasmas. The viability of long, high bootstrap current fraction operations has been established for ELMing H mode plasmas with toroidal beta values in excess of 15% and sustained for several current relaxation times. Improvements in wall conditioning and fueling are likely contributing to a reduction in H mode power thresholds. Electron thermal conduction is the dominant thermal loss channel in auxiliary heated plasmas examined thus far. HHFW effectively heats electrons, and its acceleration of fast beam ions has been observed. Evidence for HHFW current drive is by comparing of the loop voltage evolution in plasmas with matched density and temperature profiles but varying phases of launched HHFW waves. A peak heat flux of 10 MW/m^2 has been measured in the H mode, with large asymmetries in the power deposition being observed between the inner and outer strike points. Non-inductive plasma startup studies have focused on coaxial helicity injection. With this technique, toroidal currents up to 400 kA have been driven, and studies to assess flux closure and coupling to other current drive techniques have begun.

1. Introduction

With the advent of significant levels of auxiliary heating and maturing diagnostic and operational capabilities over the last two years, the National Spherical Torus Experiment [1] (NSTX) has begun intensive research aimed at establishing the physics basis for high performance, long pulse, solenoid-free operations of the spherical torus [2] (ST) concept. This research is directed at developing an understanding of the physics of the ST operational space, developing tools to expand this space, and contributing broadly to toroidal science. To these ends, research in the last two years has focused on high beta MHD stability, confinement, high harmonic fast wave heating and current drive, boundary physics, solenoid-free startup, and exploration of scenarios that integrate favorable confinement, stability, and non-inductive current drive properties. Some results in these efforts include the following:

- Toroidal beta values ($\beta_t \equiv <p>/(B_{t0}^2/2\mu_0)$) up to 35% with neutral beam heating have been obtained. In some plasmas at high normalized beta $\beta_N \equiv \beta_t/(I_p/aB_t)$, the no-wall stability limit is exceeded by 30%.
- Pulse lengths have been lengthened to 1 second with the benefit of bootstrap and beam-driven non-inductive currents of up to 60 % of the total.
- Normalized beta values β_N up to 6.5 %·m·T/MA have been achieved, with operations overall bounded by ratios of β_N to the internal inductance $l_i = 10$.
- Energy confinement times in plasmas with both L and H mode edges exceed the ITER98pby(2) scaling [3] by over 50%, and the ITER89-P L-mode scaling [4] by over a factor of two for both discharge types.
- Particle transport studies of plasmas with turbulent (L mode) edge conditions reveal impurity transport rates that are consistent with and in some cases fall below neoclassical predictions in the core.
- Signatures of resistive wall modes have been observed [5,6]. With sufficiently broad pressure profiles, their onset occurs above the calculated no-wall stability limit, pointing to the presence of passive wall stabilization.
- Tearing mode activity consistent with the expected behavior of neoclassical tearing modes has been observed. These modes can saturate beta or cause beta reduction when the central q value is near unity, but for higher q values their effect on performance is modest.
- New classes of fast-ion-induced MHD have been observed [7,8,9]. These Compressional Alfvén eigenmodes (CAEs) exist near the ion cyclotron frequency. Bounce-precession

fishbone bursts are seen near 100 kHz, and are associated with fast ion losses.
- Significant heating of electrons with high harmonic fast waves (HHFW) has been measured [10]. Interactions between fast beam ions and HHFW have been observed.
- The first indications of current driven by HHFW have been obtained [10].
- The application of coaxial helicity injection [11,12] (CHI) has yielded a toroidal current of up to 400 kA, with observations of n=1 MHD activity that may be a prerequisite for closed flux surface formation.
- Edge heat flux studies [13] divertor infrared camera measurements indicate that 70% of the available power flows to the divertor targets in quiescent H mode discharges.

In this work, operational capability and diagnostics are described in Section 2. Section 3 summarizes three studies aimed at realizing high toroidal beta, demonstrating long pulse operations sustained by significant non-inductive current, and the combined realization of high beta and efficient confinement for durations longer than an energy confinement time. Section 4 contains summaries of topical research in MHD, confinement, HHFW, boundary physics, and coaxial helicity injection. Particular attention is given to those elements relevant to establishing the physics and operational basis for long pulse, high beta, high confinement regimes with high fractions of non-inductive current drive.

2. NSTX Device Description and Facility Capabilities

Some of the NSTX device characteristics [14] and facility capabilities are as follows. NSTX can generate plasmas with an aspect ratio R/a as low as 1.27. Plasma currents up to 1.5 MA have been obtained, and deuterium neutral beam injection (NBI) for heating and current drive is used routinely. Injected in the direction of the plasma current, the NBI system is capable of delivering 5 MW for up to 5 s. Powers up to 7 MW have been achieved for shorter periods of time. High harmonic fast wave [15] can be delivered at variable phase for heating and current drive. Injected powers up to 6 MW have been achieved. NSTX has a close fitting conducting shell to maximize the plasma beta. The toroidal field capability ($B_T \leq$ 0.6 T) allows for pulse lengths up to 5 s at lower fields. Single and double null configurations can be generated, and elongations up to 2.5 and triangularities up to 0.8 have been achieved. Finally, the inner and outer halves of the vacuum vessel are electrically isolated from each other and can be biased for studies aimed at starting and sustaining the plasma non-inductively using coaxial helicity injection (CHI) [11].

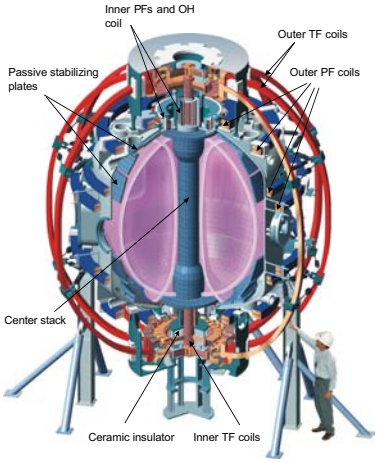

Figure 1. Schematic cut-out view of the NSTX device.

Operational developments include development of 350^0 C bakeout capability of the plasma-facing graphite tiles, implemented prior to the 2002 research campaign. This is part of a larger wall conditioning program [16] that includes routine application of helium glow between shots to reduce impurity influxes, as well as boronization every few weeks of operation or as deemed necessary. Minimization of error fields by realignment of an outer poloidal field coil last year reduced the frequency of the onset of locked modes, widening the NSTX operating space. Finally, the capability of fueling the plasma from the center stack was implemented, motivated by work on the MAST device [17], complementing the outboard gas puffing capability. One result of these improvements was improved access to and reproducibility of H modes.

A schematic cross section of NSTX is shown in Figure 1 [18,19]. Central to NSTX research is a suite of diagnostics [20], including a multitimepoint Thomson scattering system (presently 20 radial points, covering high field side to low field side, at up to 60 Hz sampling) that is absolutely calibrated for both density and temperature profile measurements. Carbon ion temperature and toroidal rotation measurements are made using charge exchange recombination spectroscopy (CHERS), with a time resolution of 20 ms (10 ms for the upcoming run period) and 17 radial channels (up to 50 channels for the upcoming run) spanning the outer half of the plasma cross section. These measurements are facilitated by a dedicated background view for direct subtraction of contaminating background. Ultra soft x-ray measurements made using three arrays, displaced toroidally and poloidally, enable core MHD instabilities to be identified. An array of magnetic sensors on the center stack, as well as the outboard side of the plasma, permit magnetic equilibrium reconstruction and identification of toroidal number of external modes. A fast magnetic coil sensor system enables measurements of MHD perturbations at several times the ion cyclotron frequency (up to 10 MHz), in the range of compressional Alfvén eigenmodes [8]. A scanning neutral particle analyzer measures the fast ion distribution function, including distortions induced by fast ion absorption of high harmonic fast waves energy. Infrared cameras have enabled the first studies of edge heat flux scalings.

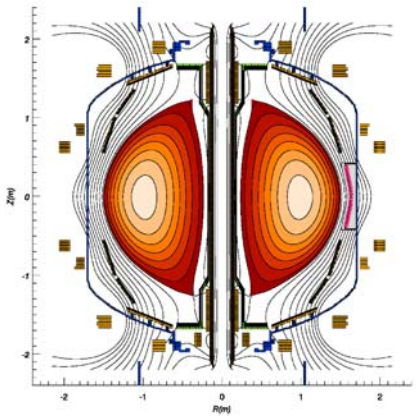

Figure 2. Surfaces of constant magnetic flux for a neutral-beam heated plasma with a toroidal beta of 35% (shot 108989). The plasma had an applied toroidal field of 0.3 T, aspect ratio of 1.4, elongation of 2.0, triangularity of 0.8.

Key to progress in research on NSTX has been the development of a flexible shaping and position control system. High triangularity and elongation raises the edge q for a fixed current and toroidal field. Owing to the strong in-out variation of the toroidal field, the shaping can be particularly beneficial to low aspect ratio devices such as NSTX, including the realization of higher values of I/aB as compared to those achievable on larger aspect ratio devices. Strong shaping also enables rapid current ramps, with typical ramp rates of up to 5 MA/s utilized at the start of an NSTX pulse. Figure 2 shows the plasma equilibrium for the NSTX discharge with a toroidal beta of 35%. The equilibria are evaluated from magnetics-based equilibrium reconstructions using the EFIT code [21]. Recently, a control algorithm based on real-time EFIT (rtEFIT) [22] reconstructions, originally developed at DIII-D, has been implemented. This will enable improved position, shape, and feedback control in future experimental campaigns.

3. High beta, long pulse, and high confinement plasmas

3.1 High beta operations - The low aspect ratio and strong shaping capability on NSTX has enabled the realization of high beta plasmas. Shown in Figure 3 are time traces from the plasma with the highest β_T yet obtained. Run in the double null configuration at 0.3 T, this plasma reached β_T of 35%. The maximum β_N was 6.3, below the no-wall limit. This discharge entered a dithering H mode state near 230 ms, which transited to an ELM-free state after 260 ms. Beta saturation was associated with the onset of an internal 1/1 mode. Depletion of available volt-seconds led to the termination of this discharge.

3.2 Long pulses with significant non-inductive current - One important goal for ST research in the long term is the achievement of high fractions on non-inductive current drive. Progress towards this has been realized through the generation of plasmas with a non-inductive current fraction of up to 60%, sustained for a duration on the order of a current penetration time (Figure 4). In these 0.45 T, 800 kA plasmas, β_T = 15 – 20%. DCON [23] analysis indicates that this plasma, with β_N of about 6, was well above the no-wall stability limit, suggesting that passive wall stabilization played a role in its sustainment. Neutral beam current drive and bootstrap currents yielded low surface voltage of 0.1 V for a time period on the order of the estimated current relaxation time of about 200 ms. Calculations indicate that late in the low loop voltage phase, more than half of the non-inductive current comes from the bootstrap effect. The total pulse lengths for these neutral-beam-heated H-mode plasmas extends to one second, with 700 ms current flattops. Early neutral beam heating and the rapid current ramp combined to reduce the plasma's internal inductance by yielding comparatively high edge current densities and slow current diffusion rates in the early phase of the discharge. Also, the development of an increased edge bootstrap current is calculated to be associated with the H mode edge pedestal.

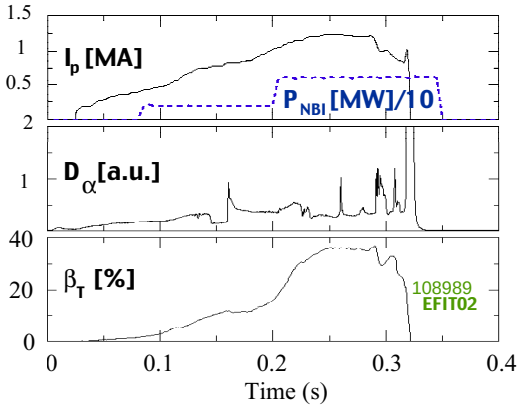

Figure 3. (a) Plasma current and NB power, (b). D_α emission, and (c) β_T for a double-null plasma. The plasma had an applied toroidal field of 0.3 T, aspect ratio of 1.4, elongation of 2.0, triangularity of 0.8, internal inductance of 0.6, and a central q as determined from magnetics analysis of 1.4

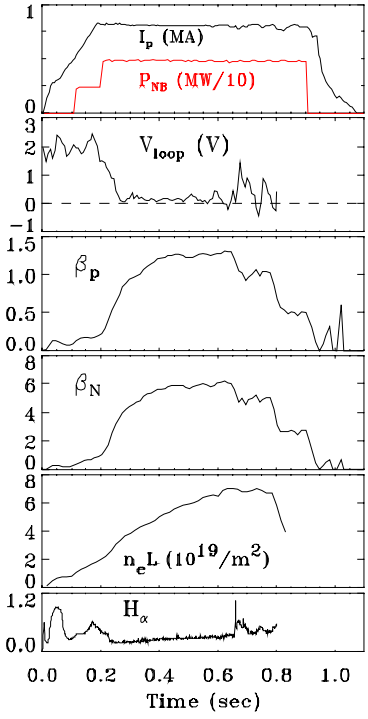

Figure 4. The plasma current, injected beam power, surface voltage, beta poloidal, normalized beta, line density, and D_α emission for an NSTX discharge with over 50% non-inductive current drive. The plasma transited to H mode shortly after the addition of the second neutral beam

The pulse length was not limited by flux consumption. Rather, MHD activity at 650 ms that appears to be related to the q profile and pressure profile evolution initiated the first drop in core beta. The details of this MHD are still under investigation. Measurements of core MHD activity with soft x-ray arrays are consistent with the hypothesis that a double tearing mode that follows the generation of magnetic shear reversal is responsible for the degradation. Confirming this awaits a direct measurement of the magnetic shear. As for increasing the performance and pulse length of these plasmas, success in combining effective HHFW with neutral beam heating could have significant impact on the plasma resistivity and bootstrap current. Modification of the q profile evolution with HHFW in this manner, and ultimately with HHFW aimed at direct current drive, represents a major research thrust for NSTX in the upcoming research campaign.

3.3 Simultaneous achievement of high stored energy and high confinement - Higher toroidal field operations led to the highest stored energies yet achieved in NSTX (Fig. 5), and

the highest combined products of beta and confinement enhancement factor. These plasmas had an applied toroidal field of 0.55 T, higher than that used in the highest beta plasmas and near the operational limit of 0.6 T. For this plasma, $\beta_N H_{89L}$, where H_{89L} is the ratio of the measured confinement time to that predicted by the ITER L mode scaling relation, is 12 or higher for 8 energy confinement times, illustrating that high performance can be maintained on NSTX for durations sufficient for the study of the physics of high beta, high confinement regimes.

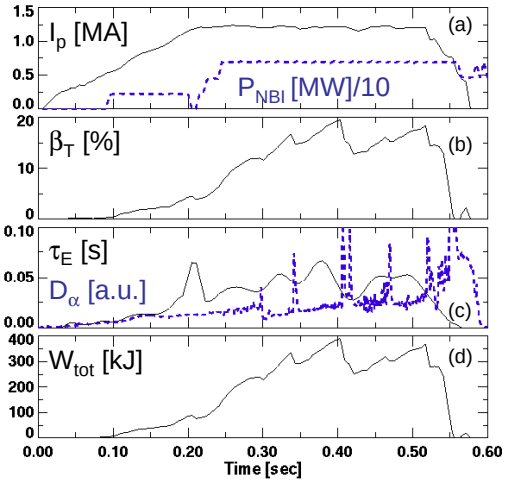

Figure 5. Data for a plasma that obtained 390 kJ of stored energy. An H mode transition occurred at 300 ms. (a). Plasma current and neutral beam heating power. (b). Toroidal beta. (c). Energy confinement time and D_α emission. (d). Stored energy, determined from analysis of magnetics data.

4. Topical Research

4.1 MHD

4.1.1 Beta limiting modes - The simultaneous realization of high values of normalized beta and low internal inductance is one component of demonstrating the attractiveness and viability of wall-stabilized, high bootstrap fraction operations of the spherical torus [24]. Research on NSTX in 2001 and 2002 has extended the range of β_T, β_N, β_N/l_i, and pulse length achieved in a toroidal confinement device of this scale. These plasmas states have been achieved with confinement times that meet or exceed expectations based on scaling laws developed from moderate aspect ratio tokamak experiments in both the L or H mode regime, as described in Section 4.2.

Some aspects of the operating space realized thus far on NSTX are illustrated in Figure 6. At present, this operating space is bounded at $\beta_N/l_i = 10$. One targeted operating point for NSTX plasmas is characterized by β_N of 8 at l_i of 0.2 – 0.3 and is based on an assumption of broad pressure profiles so as to maximize the bootstrap current and stability. Achieving the highest values of β_N simultaneously with the lowest values of internal inductance demands that NSTX operate beyond the no-wall stability limit. However, a challenge is to find a path to these configurations. It is only for $\beta_N > 5$ or more that global MHD modes exhibit magnetic perturbations with poloidal wavelengths sufficiently long for effective wall coupling. To date, the path that has most successfully led to this corner of the NSTX operating space has utilized rapid current ramps, early neutral beam heating, shaping, and transitions to the H mode that yield broad pressure profiles. H mode pressure profiles also have benefits with respect to ideal stability, bootstrap current generation, and large plasma volume with high energy content. It

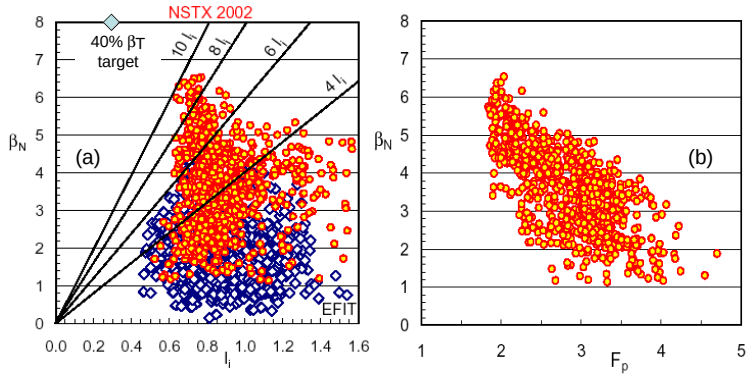

Figure 6. The achieved values of (a) β_N vs. plasma internal inductance, and (b) β_N vs. pressure peaking factor for NSTX in the 1999 through 2002 research campaigns. The lighter points are data obtained in the 2002 campaign. Beta and internal inductance is determined with EFIT code analysis of magnetics data.

should be pointed out, however, that plasmas with L mode edges in NSTX also exhibit high confinement and toroidal beta values that approach or even exceed 30%.

Analysis of many plasmas with high β_N indicate that the no-wall stability limit has been exceeded, and that wall stabilization is likely a critical player in achieving this state. Shown in Figure 7 are β_N and the central rotation for a discharge that exceeds the no-wall stability limit as calculated by the DCON code. The no-wall limit is surpassed for several wall times. Significantly, the collapse of high plasma stored energy and falling below the no-wall limit is preceded by a reduction of the plasma rotation, suggesting that the wall mode stabilization that is enabled by this rotation is lost at some critical rotation frequency. A detailed analysis of passive wall stabilization in high β_N NSTX plasmas is provided in Ref. [6].

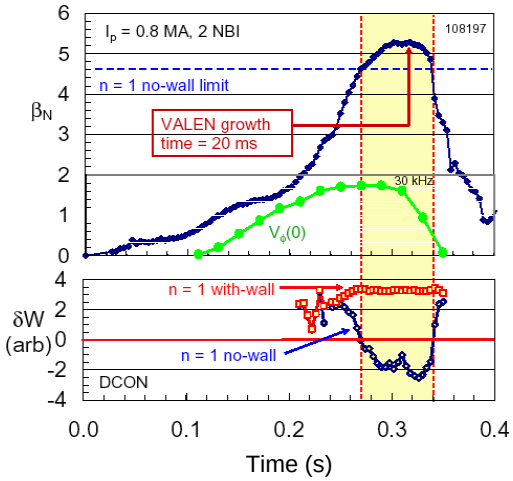

Figure 7. β_N and central carbon rotation velocity as a function of time. This plasma exceeds the no-wall stability limit, as identified by the DCON code, for several wall times. The loss of stability is preceded by a reduction of the plasma rotation.

Tearing mode activity, probably neoclassical tearing modes, have been observed on NSTX to saturate beta in some cases, as well as to degrade overall performance. These modes are slowly growing and, in many shots, are identified as 1/1, 2/1, and 3/2 islands. The mode growth is consistent with that predicted by modified Rutherford equation. These modes are most easily avoided by operating plasmas with elevated q(0), which is consistent with the desired final high performance state of low internal inductance operation.

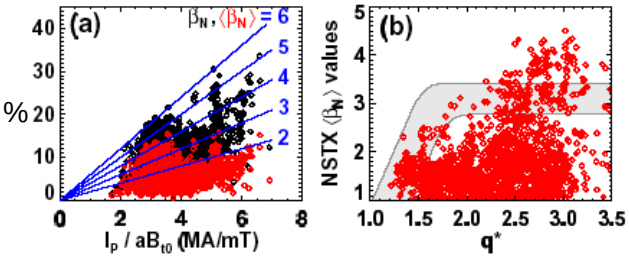

Figure 8. (a) β_T (black) and $<\beta>$. (red) at maximum stored energy for NBI-heated plasmas plotted versus normalized current. Constant β_N lines are shown (b) $<\beta_N>$. versus q for the discharges from (a). From Ref. 25.*

A recent theoretical study [25] reveals that the theoretical ideal beta limits of moderate aspect ratio tokamaks and ST's can be viewed in a unified fashion if the standard definition of beta is broadened. It is found that the normalized beta limits over a wide range of aspect ratio are similar if the volume-averaged magnetic field pressure $<\beta> \equiv 2\mu_0<p>/<B^2>$ is used to define $<\beta_N> \equiv <\beta(\%)aB_{t0}/I_p(MA)$, where B_{t0} is the applied vacuum magnetic field. Figure 6 shows a database of normalized beta values using both the usual definition and this modified definition. The shaded band in Figure 8 shows the stability limit for moderate and small aspect ratio achieved in the theoretical study, along with the NSTX data. These plasmas exceed this theoretical limit, suggesting that some stabilization mechanism is at work.

4.1.2 Fast beam-ion-induced MHD - In general, ST's are susceptible to fast ion driven instabilities due to the relatively low toroidal field. Indeed, a wide variety of such instabilities has been seen in NSTX at frequencies ranging from a few kHz to many MHz [9]. In the frequency range below about 200 kHz, a form of the fishbone or energetic particle

mode has been seen, as well as modes that appear to be similar to the TAE modes of conventional tokamaks. Unlike in conventional tokamaks, the frequency ranges of these two classes of instabilities have substantial overlap, complicating the experimental identification and theoretical analysis. Significant fast ion losses have been correlated, under some conditions, with the appearance of both of these types of modes.

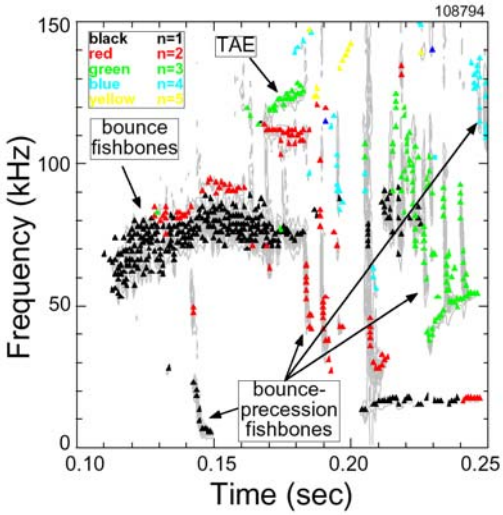

Figure 9. A sampling of the energetic particle modes often observed an NSTX neutral-beam-heated discharge.

In the higher frequency ranges, up to 5 MHz, or perhaps higher, observed modes may be related to the various forms of Ion Cyclotron Emission (ICE) of conventional tokamaks. According to theoretical modeling, that both Global Alfvén Eigenmodes (GAE) and Compressional Alfvén Eigenmodes (CAE) could be destabilized by the fast ion population. There is some experimental/theoretical evidence that both have been observed on NSTX. Their presence could clearly impact fast ion distributions and thus, ultimately, fast ion confinement, but no clear experimental evidence exists for this as yet.

An experiment has been performed in conjunction with the DIII-D tokamak that takes advantage of the similar cross-sectional shapes and area, but different aspect ratios. Toroidal Alfvén Eigenmodes (TAE) modes were identified at similar frequencies in both but at higher mode numbers on DIII-D, as expected by theory. Also, the threshold in beam beta for beam-driven instabilities is similar in both devices.

4.2 Confinement and transport

4.2.1 Global Confinement – The confinement times in neutral beam heated NSTX plasmas compare favorably to the ITER-89P empirical scaling expression as well as the ITER-98(pby,2) scaling rule [26,27]. This is true for plasmas with distinct H mode transitions as well as for L mode edge plasmas. An interesting aspect of this relation between the H and L mode states can be seen in Figure 3. At the H mode transition (near 230 ms), a change in plasma beta and stored energy is not noticeable. While an increase in the rate of change of stored energy is usually observed in L to H transitions, these other cases are prompting analysis of the local changes of transport properties in the core and edge across an L to H mode transition.

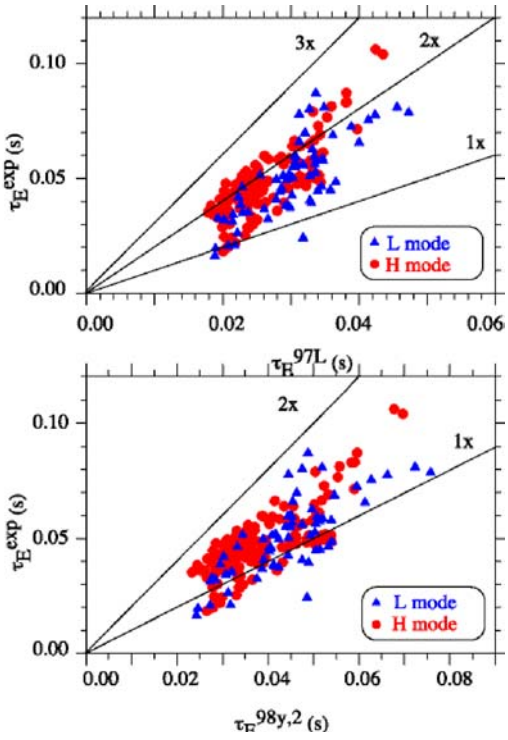

Figure 10. Energy confinement times, determined with magnetics analysis, compared to values calculated from the two ITER scaling expressions. Data for plasmas with both L and H mode edges are shown.

4.2.2 H mode access, dynamics, and power balance - H mode operations have become routine on NSTX, aided by improved wall conditioning and reduced error fields. Access to

the H mode is easiest in the lower single null configuration, but H modes have been obtained in double null as well. The power threshold of several hundred kW in some cases and is exhibiting a secular fall as wall conditions improve [28].

The evolution of the density of the long-pulse H mode plasma described can be seen in Figure 11. Of note is the presence of pronounced "ears" in the electron density profile that arise shortly after the L to H transition, likely a signature of an edge particle transport barrier.

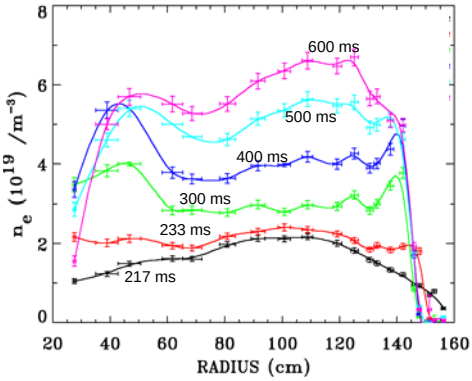

Figure 11. Density evolution in the long-pulse H mode described in Figure 4.

A time slice of the profile measurements of the electron temperature T_e, the ion temperature T_i, and the rotation velocity V_ϕ are shown in Figure 12. The high T_i compared to T_e is a persistent feature seen in most NSTX neutral-beam-heated discharges. Along with expectations that neutral beam fast ion energy should be transferred predominantly to the electrons in this temperature range, this suggests that the dominant loss channel is electron thermal conduction. This is indeed born out in the power balance analysis, which shows ion thermal conductivity χ_i that are on the order of predictions from neoclassical theory, and electron thermal conductivity χ_e that is significantly larger than χ_i. The momentum diffusivity χ_ϕ is smaller than χ_i in this analysis, qualitatively consistent with expectations from neoclassical theory. Analysis of neon gas puffing also suggests that the impurity diffusion is near neoclassical levels in the core of L mode plasmas. Microinstability analysis of beam-heated plasmas using the GS2 gyrokinetic code [29] is being performed to assess the roles of long wavelength ion temperature gradient (ITG) and trapped electron (TEM) modes, as well as shorter wavelength electron temperature gradient (ETG) modes. Further details of NSTX core confinement studies can be found in Ref. [30]

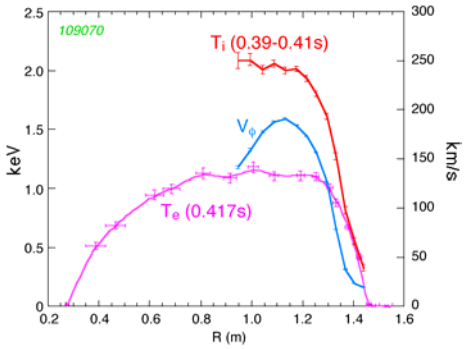

Figure 12. T_i, T_e, and toroidal rotation V_ϕ in the long pulse H mode discharge described in Figure 4.

4.2.3 Edge turbulence measurements – Three different measurement techniques have been implemented to measure turbulence characteristics in the plasma scrapeoff layer. All of them – an edge reciprocating Langmuir probe, edge reflectometry, and gas puff imaging – reveal highly turbulent SOL activity in the L mode. The edge probe and imaging point to the presence of intermittent convective transport events. These results will be compared to developing theory of these nonlinear transport phenomena. Studies will focus on assessing their role in determining the overall radial heat transport to the divertor.

4.3 High Harmonic Fast Wave Heating and Current Drive - Over the last two years, a campaign to explore the physics and the application of high harmonic fast wave (HHFW) heating has been carried out on the NSTX device with the ultimate goal of providing a tool for long pulse, high beta ST operation. RF wave energy is launched into the NSTX plasma at a frequency of 30 MHz via a twelve-element antenna array. The elements can be phased to launch a variety of wave spectra with toroidal wave numbers between ±14 m^{-1}.

As expected from theory, electron heating has been observed for a wide variety of plasma

conditions and over the full range of applied wave spectra. Electron temperatures as high as 3.7 keV have been produced. Heating efficiency, characterized by the value of the central electron temperature, seems to be highest for the slowest wave phase velocities. NSTX plasmas with predominantly electron heating exhibit a strong degradation in confinement, which is consistent with theoretical predictions of an increase in conduction due to ETG modes. Attempts to measure the power deposition profile with modulated rf power have also showed a very stiff temperature profile response consistent with a marginally stable profile. Some discharges are characterized by an apparent barrier in the T_e profile, and by reduced electron conduction in the central region. Long duration, 400 ms, steady rf driven H-modes at moderate plasma current I_p =350 kA with β_p near unity, and bootstrap current fraction of 40% have been created. These H-modes have continuous ELM activity and are not accompanied by a strong increase in density or Z_{eff}. H modes at higher values of plasma current have been ELM-free, with steadily increasing density until the termination after only a brief, ~40 ms interval.

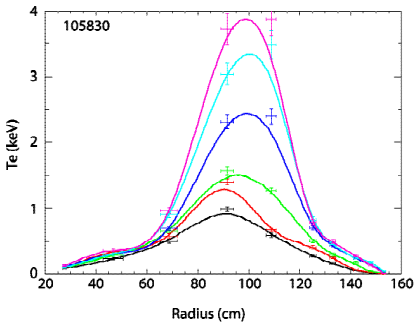

Figure 13. Electron temperature for a plasma heated with 3.5 MW HHFW over a 100 ms time interval.

Experiments with directed wave spectra have been conducted to investigate the possibility of driving plasma current. Differences between co and counter directed HHFW waves have been observed in the loop voltage (Fig. 14) and in the MHD behavior, which are consistent with current being driven on axis in the expected direction. Careful matching of the electron temperature and density are required to make meaningful comparisons between the shots. For the best-matched cases at ± 7 m^{-1} a driven current of about 100 kA is inferred from the loop voltage, in reasonable agreement with predictions from the TORIC code [31] and a factor of two smaller than that estimated from CURRAY [[32]]. Loop voltage differences have also been observed for faster wave phase velocities down to ±2.4 m^{-1}. An interesting and not understood effect is that differences in central heating efficiency are also found between co and counter phasing with counter up to twice as efficient. Theory predicts no substantial difference in heating efficiency for the opposed spectra.

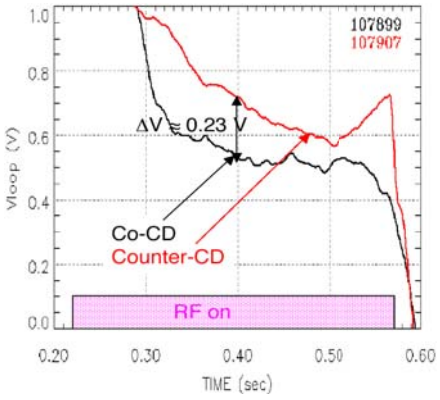

Figure 14. Surface loop voltage for two HHFW-heated plasmas with co- and counter antenna phasing. The n_e and T_e profiles were matched by adjusting the heating power to be 2.2 MW co-phasing, 1.2 MW counter phasing.

Ion heating provides a potential alternate channel for rf absorption that can lower the efficiency of current drive. Despite the large values of cyclotron harmonic involved (9-14), significant wave damping is expected at large values of the ion beta. Acceleration of neutral beam injected 80 keV ions to 140 keV has been observed. The ion tail is strongest at the highest values of toroidal field. It also shows a small dependence on wave spectrum, decreasing for increasing phase velocity in contrast to theoretical predictions of the opposite behavior. No dependence on plasma current was observed and the observed dependence on injection energy shows a smaller interaction at lower voltage.

4.4 Boundary physics – Boundary physics research in NSTX focuses on power and particle balance. High heat flux on the target plate has been measured in lower-single null (LSN)

divertor plasmas. For example, the peak heat flux in a lower single null ELM-free H-mode plasmas with 4.5 MW of heating power has reached 10 MWm^{-2}, with a full-width half-max of 2 cm at the outer target plate [28], approaching the spatial resolution of the IR camera used to make the measurement (Fig. 15). Peak heat flux in H-mode plasmas increases with NBI heating power. The peak heat flux at the inboard target is typically 0.5 – 1.5 MW/m^2, with a profile full-width half max. of ~ 10 cm. The power flowing to the inboard side is typically 0.2 – 0.33 of the outboard power (Fig. 15). Outer target tile heating and incident power appear to be higher in L-mode plasmas than ELM-free H-mode plasmas, whereas the inboard sides are comparable.

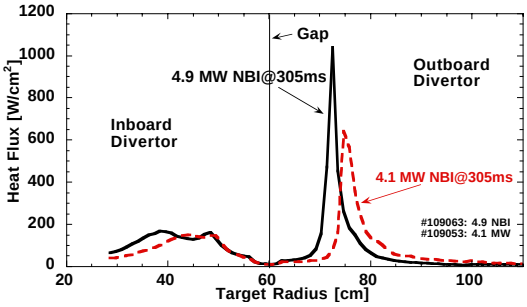

Figure 15. Divertor heat flux in two quiescent H modes, one with 4.1 MW injected NB power, the other with 4.9 MW

A tile temperature increase of 300 °C has been measured during the first 0.2 s after divertor establishment in H-modes; extrapolation of the temperature rise, assuming an increase ~ $(\text{time})^{1/2}$ with constant peak heat flux, yields a tile temperature in excess of the 1200 °C engineering limit after ~ 3 s. While this limitation should not impact the NSTX near-term program of investigating pulse lengths up to several energy confinement times, more detailed study is required to assess the power handling requirements for pulse lengths in excess of several current penetration times (beyond 1 second) at the highest available input powers. As pulse lengths are increased in NSTX, the emphasis in boundary physics research will be placed on using double-nulls, radiative divertor/mantle solutions, and X-point sweeping.

4.5 Coaxial Helicity Injection - Strategies for initiating current non-inductively on NSTX by the process of coaxial helicity injection (CHI [11,12]) are being developed. CHI is implemented on NSTX by driving current along field lines that connect the inner and outer lower divertor plates. A description of the CHI system on NSTX can be found in Reference [33].A 50kA, 1kV DC power supply is connected across the inner and outer vessel components, which are insulated from each other by ceramic rings at the bottom and top. The CHI method drives current initially on open field lines, creating a current density profile that is hollow and intrinsically unstable. Taylor relaxation predicts a flattening of this current profile through a process of magnetic reconnection leading to current being driven throughout the volume, including closed field lines.

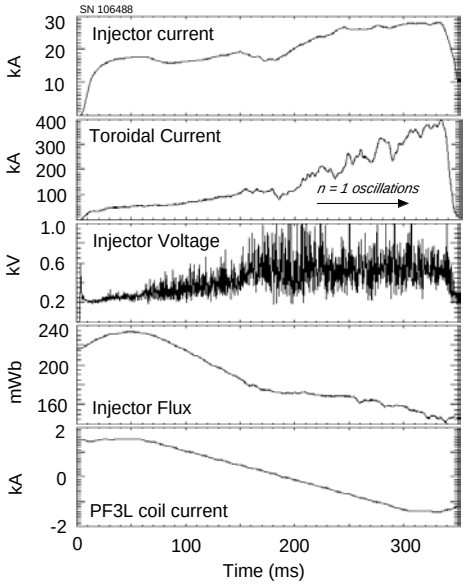

Figure 16. Injector parameters, and toroidal and coil current in a CHI discharge

The applied injector voltage determines the amount of injector current that can be driven for each combination of toroidal field, injector flux and gas pressure. This flux is defined as the difference in poloidal flux between the upper and lower insulating gaps separating the inner and outer electrodes. In this discharge shown in Figure 16, as the injector voltage is increased and the injector flux reduced, the toroidal current reaches nearly 400kA. The injector current is 28kA, which results in a current multiplication factor of 14, roughly equal to the theoretical maximum attainable. During the high current phase after 200 ms, there are oscillations in the toroidal current signal. It is not known if these are signatures of

reconnection events that lead to closed flux plasma that then decays, only to be re-established. In high current discharges such as this, a magnetic perturbation with amplitude $2mT$ measured at the outboard midplane and toroidal mode number $n=1$ is observed, rotating toroidally in the $E_r \times B_p$ direction with a frequency in the range $5 - 12kHz$. Such a mode, which has been seen on high current CHI discharges on HIT and HIT-II, may be a signature of the formation of closed flux surfaces.

Plans on NSTX are to produce higher current, longer discharges for characterization with and without auxiliary heating. To this end, the absorber region has been modified to suppress arcs, and feedback control should help to retain the closed flux that may be created in future higher current CHI discharges, a necessary step in performing a successful handoff to other current drive scenarios. A new short pulse discharge initiation method, developed on HIT-II, will be used on NSTX to hand-off a CHI discharge for inductive operation [34].

Summary: This research was supported by DoE contract DE-AC02-76CH03073.

[1] M.Ono, Proceedings of the 18th IAEA Meeting, Sorrento, Italy, 2000.
[2] Y-K M. Peng, and D. J. Strickler, Nuclear Fusion **26** (1986) 576
[3] The ITER Team, *Nucl. Fusion* **39** (1999) 2137.
[4] P.N. Yushmanov *et. al.*, *Nucl. Fusion* **30** (1990) 1999.
[5] S. Sabbagh *et al.*, Nucl. Fusion **41** (2001)1601.
[6] S. Sabbagh *et al.*, paper EX/S2-2, this conference.
[7] N.N. Gorelenkov and C.Z. Cheng, C.Z., Nucl. Fusion **35** (1995) 1743.
[8] E.D. Fredrickson, N.N. Gorelenkov, C.Z. Cheng *et al.*, Phys Rev. Lett. **87** (2001) 145001.
[9] D. Gates, R. White, N. Gorelenkov, Phys. Rev. Lett **87** (2001) 205003.
[10] P. M. Ryan, paper EX/P2-13, this conference.
[11] T.R. Jarboe, *et al.*, Phys. of Plasmas **5** (1998) 1807-14
[12] T.R. Jarboe *et al.*, *Proceedings of the 17th IAEA Fusion Energy Conference*, Yokohama, IAEA-CN 69/PDP/02 (1998).
[13] R. Maingi *et al.*, in *Proceedings of the 11th International Conference on Plasma Physics* (Sidney, Australia, 2002), Plasma Phys. Control. Fusion (in press).
[14] M. Ono *et al.*, in Proc. *18th IEEE/NPSS Symp. On Fusion Enginnering*, Albuquerque, 1999, IEEE, Piscataway, NJ (1999) **53**.
[15] M. Ono Phys. Plasmas **2** (1995) 4075.
[16] H.W. Kugel *et al.*, *J. Nucl. Mater.* **290-293** (2001) 1185.
[17] A. Sykes, et al., in Plasma Phys. Control. Fusion (1994) (Proc. 15th Int. Conf. Seville, 1994) **1**, IAEA, Vienna (1995) 719.
[18] C. Neumeyer *et al.*, in *Proc. 18th IEEE/NPSS Symp. On Fusion Engineering*, Albuquerque, 1999, IEEE, Piscataway, NJ (1999).
[19] J. Chrzankowski, *et al.*, ibid.
[20] R. Kaita *et al.,* in the Proceedings 28th International Conference on Plasma Science (ICOPS) / 13th International Pulsed Power Plasma Science (PPPS-2001), Las Vegas, Nevada, June 17 - 22, 2001.
[21] L. Lao *et al* Nucl. Fusion **30** (1990) 1035
[22] J.R. Ferron *et al.*, *Nucl. Fusion*, **38** (1998) 1055
[23] A. H. Glasser and M. S. Chance, Bull. Am. Phys. Soc. **42**, 1848 (1997).
[24] J. E. Menard, S. C. Jardin, S. M. Kaye *et al.*, Nucl. Fusion **37** 595 (1997)
[25] J. Menard *et al.*, submitted to Phys. Rev. Lett.
[26] Kaye S. *et al.,* Nucl. Fus. **37** (1997) 1303
[27] The ITER Team, Nucl. Fus. **39** (1999) 2175.
[28] R. Maingi *et al.*, paper EX/C2-5, this conference.
[29] M. Kotschenreuther *et al.*, Comp. Phys. Comm. **88** (1995) 128.
[30] B. LeBlanc *et al*., paper EX/C5-2, this conference.
[31] M. Brambilla, Plasma Phys. Control. Fusion **41** (1999) 1.
[32] T.K. Mau et al., Proc. of the 13th Top. Conf. on Applications of RF Power to Plasmas, Annapolis, Maryland (American Institute of Physics, Melville, 1999) 148.
[33] R. Raman *et al*., *Nucl. Fusion* **41** (2001).1081
[34] R. Raman *et al.*, submitted to Phys. Rev. Lett.